Electric Field Modulated Near-Field Photo-Luminescence of Organic Thin Films

David M. Adams, Josef Kerimo, Chong-Yang Liu, Allen J. Bard, and Paul F. Barbara*

Department of Chemistry, University of Texas at Austin, Austin Texas 78712

Received: December 23, 1999; In Final Form: May 17, 2000

The concentrated electric field (E-field) in the vicinity of a *voltage-biased* near-field optical probe is used to modulate the photoluminescence of organic thin films on the ∼100 nm scale. The samples are bilayers comprising a self-organized-thin-film (50−500 nm) layer of zinc-octakis (*β*-decoxyethyl) porphyrin (ZnODEP**)** on top of an indium tin oxide (ITO) coated glass electrode. The Al coated-optical-fiber-near-field probe functions simultaneously as a noncontacting moveable electrode and a local source of optical excitation (30−70 nm aperture). When the ITO electrode is charged positive relative to the probe (yielding a field on the order of $1MV/cm^{-1}$), the photoluminescence (fluorescence) intensity decreases ∼5% and the probe−sampleprobe−sample distance (under shear-force feedback control) increases ∼7 Å. Opposite effects for both signals occur when the ITO is charged negative. The E-field effect on the near-field luminescence properties of thin films of ZnODEP is discussed in terms of the following physical mechanisms: (i) direct field induced dissociation of excitons, (ii) exciton/charge carrier electron/hole transfer processes, and (iii) interfacial electron/hole transfer processes. The potential for using the observed effects as an indirect means of imaging charge injection efficiencies in organic thin film devices is explored.

Introduction

There is growing interest in the underlying physical processes in optoelectronic devices based on organic materials, including flat panel light emitting displays, solar cells, optical-electronic memories, and fluorescent chemical sensors.[1] Such devices are composed of multilayer structures, involving layers of nanostructured organic polymeric and crystalline materials, as well as inorganic layers, especially the commonly used optically transparent electrode, indium tin oxide (ITO). One of the major issues in this area of research is the impact of the layer and interfacial morphology on the essential physical processes, such as charge injection at the interfaces, charge and exciton mobilities, and exciton decay processes.[2−6] Several techniques exist for the determination of morphology, including low angle X-ray diffraction, electron microscopy, atomic force microscopy, scanning tunneling microscopy, and near-field scanning optical microscopy.[4]

There is a need, however, for experimental tools that allow for imaging (spatial resolution) of the physical processes associated with device function. Ideally, simultaneous imaging of the layer morphology and physical processes would ultimately allow *for a direct correlation of morphology and device physics in a functional device and device prototypes*. A few reports of local measurements of device physics have been made, including the use of metallized STM probes as liftable electrodes for excited electroluminescence in Al(tris-quinolate) thin films,[7] AFM probing of conductivity in electroluminescent alpha sexithiophene,[8] STM probing of the structure and electronic properties of nanowires,[9] NSOM probing of E-field induced molecular reorientation in liquid crystal display materials,[10] and STM measurements of high-density memory storage in Zn porphyrin charge trapping materials.[5,11,12]

In this paper, we investigate spatially localized E-field modulated photoluminescence spectroscopy as a technique for probing local device physics. We use the concentrated E-field in the vicinity of an *electrically biased* near-field optical probe to modulate the photoluminescence (fluorescence) of organic thin films on the ∼100 nm scale. A similar configuration was used to produce Stark shifts in the fluorescence excitation spectra of an organic system at cryogenic temperatures.[13]

Nonspatially resolved E-field modulated photoluminescence spectroscopy (with large parallel planar electrodes) has been extensively used to investigate the electrooptic behavior of organic materials, such as molecular photoconductors,[14,15] molecular LED materials,[16] and fluorescent conjugated polymers.[17−23] Organic thin films of these materials exhibit efficient E-field-induced photoluminescence quenching, as large as 75%, for fields approaching 4.5MV/cm.[23] *Field-induced dissociation of singlet excitons,* S_1*, into charge carriers (i.e., postive,* P^+*,* and negative polarons, P^-*) by the applied E-field* (eq 1) is believed to be one of the important fluorescence quenching mechanisms.

$$S_1 \rightarrow P^+ + P^- \qquad (1)$$

The mechanism may, however, be considerably more complex because the photoconductivity data indicate that intermediates, such as geminate pairs of carriers, may be involved in the formation of free charge carries.[21] The field-induced quenching data have been analyzed to determine singlet excitons binding energies E_B, which are found to significantly greater than k_BT. For example, in the case of the conjugated polymer, poly-(phenyl-*p*-phenylene vinylene) $E_B \cong 0.4$ eV.[17]

Induced nonradiative decay of singlet excitons by either positively or negatively charged polarons ($P^{\pm}$*)* in the organic layer is another important field-induced quenching mechanism.[17,18,20] This process is especially important when the device contains a large space charge due to polarons, such as in a forward biased LED above the forward conduction threshold. A microscopic picture for the mechanism has not been established. It may involve dissociation of excitons by the intense local fields of the polarons (eq 2), a direct electron-

10.1021/jp994457a CCC: $19.00
Published on Web 06/29/2000

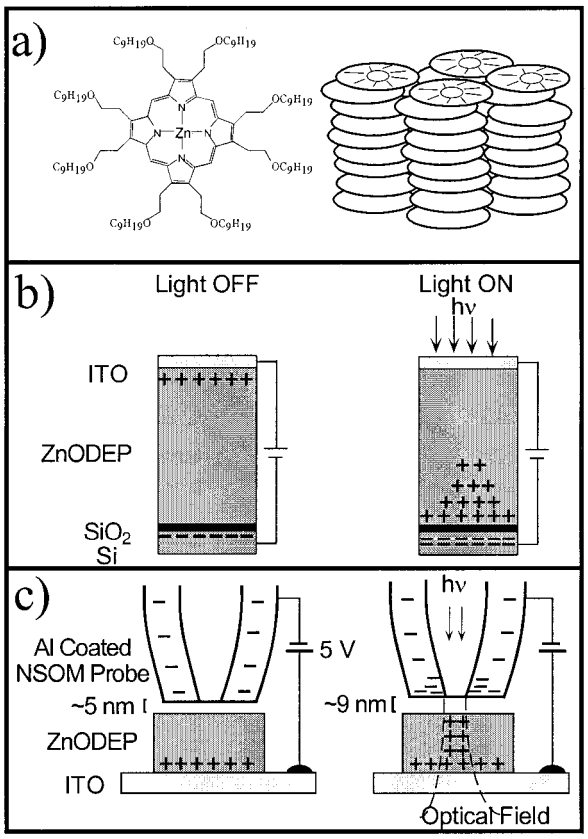

Figure 1. (a) Molecular structure of ZnODEP and proposed model of molecular stacking with some defects along the stacks. (b) Charge trapping photocapacitive device composed of ITO/ZnODEP/SiO_2/Si layer structure and proposed model of charging under illumination. (c) Device equivalent structure composed of ITO/ZnODEP/impurity-layer/Al-Coated Near-Field Probe.

transfer mechanism (eq 3) or an energy transfer mechanism (eq 4) in which $P^{\pm}$ is excited to a midgap state by the energy transfer process.

$$S_1 + P^{\pm} \rightarrow P^{+} + P^{-} + P^{\pm} \quad (2)$$

$$S_1 + P^{\pm} \rightarrow P^{\pm} + S_0 \quad (3)$$

$$S_1 + P^{\pm} \rightarrow S_0 + P^{\pm,*} \quad (4)$$

In this first report of spatially localized E-field modulated photoluminescence, we investigate the photoconductive material, zinc-octakis (β-decoxyethyl) porphyrin (ZnODEP) (Figure 1a), which has been employed in photocells and optical memory charge trapping devices composed of a thin film of ZnODEP sandwiched between two electrodes.[5,11,12,24,25] ZnODEP is crystalline at room temperature but forms discotic liquid crystalline phases at elevated temperatures. Highly organized crystalline thin films are produced by capillary filling sandwich cells (above the isotropic liquid transition temperatures) followed by cooling below the melting point.

Consider for example, the photocapacitive charge trapping device of the structure *ITO/photoconductor/SiO_2/Si*, shown in Figure 1b.[25] This device incorporates an SiO_2 insulating layer at one of the electrodes. The active photoconductive layer is a thin film of ZnODEP. The dark resistivity of the material is high ($\sim 10^{14}$ Ω-cm). However, under illumination, charges migrate in response to the E-field by photoconduction and accumulate at the SiO_2 interface. If the light is turned off after charging, the charges remain trapped due to the insulating character of ZnODEP and can be released upon illumination under short circuit conditions. Photocapacitive charge-trapping sandwich cells preferentially trap holes or electrons within the layer depending on the polarity at the illuminated electrode.[5,25] Holes are trapped when the ITO electrode is charged positive and electrons are trapped when the ITO electrode is charged negative.

In the technique described in this paper a charge trapping optical memory device is simulated in the NSOM. The device equivalent structure (Figure 1c) is *ITO(electrode)/ZnODEP-(photoconductor)/impurity-layer(insulator)/near-field probe-(electrode)*. The fluorescence intensity of ZnODEP, induced by near-field optical excitation, is observed to modulate as much as 5% as the electrical bias on the near-field probe is varied. The magnitude, direction, and dynamics of the modulation are investigated as a function of light intensity, bias voltage, sample thickness, and sample position. Additionally, variations in the interaction of the charged probe and charged sample surface are monitored by recording the z probe position, which is under shear-force-feedback control. Electric-field effects on the near-field optical and shear-force behavior are discussed in terms of the various processes that have been previously identified in the study of E-field modulated photoluminescence spectroscopy. No single mechanism, however, is able to account for the observed effects. Finally, polarized fluorescence and transmission NSOM and simultaneous scanning force microscopy are used to spatially resolve the complex morphologies and self-organized structure of thin films of ZnODEP on ITO.

Experimental Section

Sample Preparation. ZnODEP was prepared as previously described.[26] ZnODEP is crystalline at room temperature and displays liquid crystal and isotropic liquid-phase transitions at 86 and 142 °C, respectively. Thin films were prepared by heating, above the isotropic liquid transition temperature, a small amount of ZnODEP sandwiched between a transparent and conducting ITO coated glass cover slip (20 Ω/square, Metavac Corp.) and a bare glass cover slip. The sandwich construction was slowly cooled to room temperature, and the two sides were carefully separated. The ZnODEP was observed to adhere predominately to the ITO side. To prepare extremely thin films, the glass slides were pressed together while the ZnODEP was in the isotropic liquid state. In this way films with thicknesses ranging from tens of nanometers to microns were prepared in a single slide.

NSOM Experiments. NSOM measurements were made on a modified Topometrix Aurora near-field scanning optical microscope using homemade, aluminum-coated, single-mode optical fiber (3M Corp., FN−SN−3224, 633 nm) NSOM probes with subwavelength optical apertures of typically 50−100 nm. The apparatus and relevant experimental details have been described previously.[27−31] Topographic imaging was performed by maintaining the probe sample distance at ∼5 nm using the shear-force feedback technique and raster scanning the sample. The near-field probe was laterally dithered at the 6th harmonic of its primary acoustic resonance at a frequency in the range of 50−90 kHz. The shear force interaction was monitored in the usual manner utilizing a 980 nm diode laser, a split differential photodiode detector, and lock-in detection. A microscope objective with high collection efficiency (Zeiss 100X, 1.2NA) was used to collect the near-field induced fluorescence and/or transmitted light. The NSOM and correlated shear-force topography results presented in this report were observed to be highly reproducible and not subject to sample damage by heating with

the NSOM probe, electrical discharge between probe and sample, probe−sample contact, and/or photolysis of the sample.

For optical imaging, films of ZnODEP were photoexcited with unpolarized 543.5 nm (CW green Helium Neon laser, Melles Griot, 05-LGR-193), polarized 457 nm (CW Ar^+ laser, OmNichrome, 543R−A−A03), or polarized 400 nm frequency doubled output of a home-built pulsed Ti-sapphire laser pumped by an Ar^+ ion laser. To control the polarization of the exciting light, $\lambda/2$ and $\lambda/4$ plates were employed prior to the fiber coupler. The purity of the polarization of the light emanating from the tip was >15:1. The amount of light coupled into the NSOM probe was typically on the order of 0.5 mW with excitation powers at the near-field probe on the order of 1−3 W/cm^2. All of the fluorescence at wavelengths greater than 550 nm was collected at the single photon counting avalanche photodiode detectors (APDs) (EG&G Canada, SPCM 203-PQ) by spectrally filtering the laser light. In some NSOM experiments, a broad band polarizing beam splitter was used in conjunction with two APDs to monitor the polarized fluorescence from the sample. In other cases, a 50/50 nonpolarizing beam splitter combined with appropriate spectral filtering allowed for the simultaneous collection of fluorescence and transmitted light signals. Near field fluorescence spectra were collected with an imaging/spectrograph (Acton Corp., Model 150) coupled to a liquid nitrogen cooled CCD detector (Princeton Instruments LN/CCD1024E/1 and ST-130 Controller).

Electrical leads were attached directly to the near-field probe and sample substrate allowing for the application of simultaneous optical and E-fields to the material. A fine multistranded copper wire was attached ∼3 mm above end of the near-field aperture, and a small amount of silver paint was used to ensure good electrical contact between the wire and the aluminum coating on the probe. The presence of the wire did not adversely affect the shear-force feedback. A programmable function generator (Wavetek Corp. model 29) was used to apply a voltage bias between the NSOM probe and the ITO electrode. The excitation light in some cases was modulated via an acousto-optic modulator (Intra Action Corp. AOM 403R) placed prior to the fiber coupler and controlled by a second programmable function generator. Both Wavetek function generators were synchronized and controlled by a personal computer.

Probe−sample distance transients were collected simultaneously with the fluorescence transients by monitoring the control output voltage signal (BNC 9 on Topometrix ECU Electronic Control Unit) of the z-piezo of the NSOM stage. The transients were subsequently averaged to yield the average probe−sample distance transients shown. Observed modulated voltage signals were small and generally on the order of 1 mV and consequently were extremely sensitive to artifacts arising from room noise and electrical line noise. The observed kinetics were sensitive to feedback settings on the ECU and external lock-in amplifier. The transients presented in Figure 7 were obtained under identical conditions with normal operating feedback settings.

Results

ZnODEP Thin Film Morphology and Spectroscopy. Much of the data in this paper involve the optical excitation at 543.5 nm of thin films of ZnODEP on ITO and the associated measurement of the E-field modulated fluorescence properties. The electronic absorption spectrum of a nonuniform film of ZnODEP that varies in thickness from ∼50 nm to 2 μm is shown in Figure 2. There are three main absorption bands of the film: the Q(0,0) and Q(1,0) in the 500 to 600 nm region and the Soret band at ∼400 nm. Q(0,0) is the excitation to the lowest energy vibrational level of the first excited singlet state S_1 and Q (1,0) is the excitation to the first excited vibrational level of S_1.[32−34] The Soret band is the transition to S_2. These absorptions correspond to in-plane polarized $\pi-\pi^*$ charge transfer type transitions of the porphyrin ring system. For symmetric porphyrin molecules, these excited states are doubly degenerate, which follows from the equivalence of the transition dipoles in the *x*,*y* directions in the plane of the ring.[33] Splitting of the electronic transitions has been observed as a result *asymmetry* in the molecular framework, chemical binding at the apical

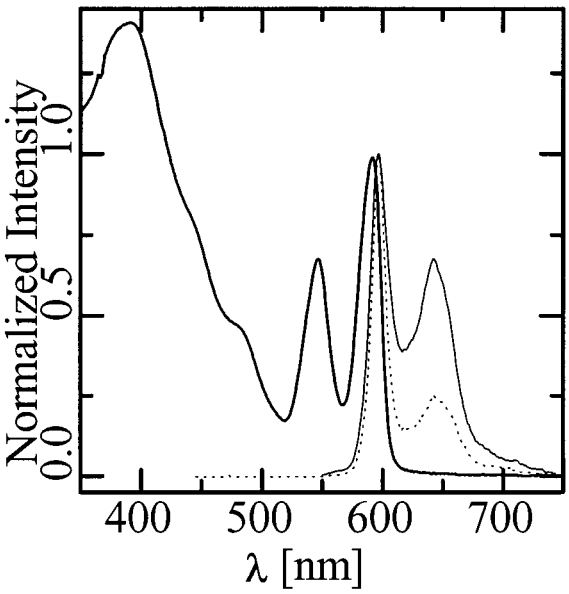

Figure 2. Far-field optical absorption and fluorescence spectra (solid-lines), and a near-field fluorescence spectrum (dotted-line) for a thin film of ZnODEP on ITO. $\lambda_{exc} = 543$ nm.

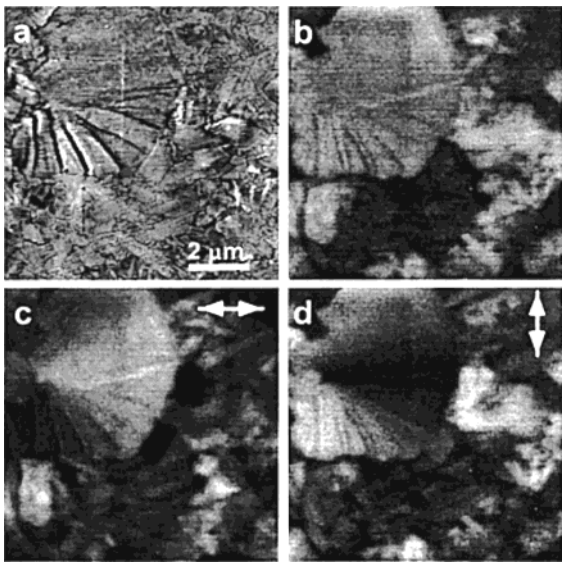

Figure 3. Topographic (a) and corresponding near field fluorescence images of a ∼ 90 nm thick film of ZnODEP on ITO coated glass where (b) is the total fluorescence and (c) and (d) are polarized fluorescence images. The sample was photoexcited with unpolarized 543.5 nm light and all fluorescence >560 nm was collected at the detectors. The polarized fluorescence images were collected with two APD detectors and a polarizing beam splitter. The direction of polarization is indicated in the images. The Z-height range in topographic image (a) is from 0 to 13 nm and the RMS roughness of the entire image is 3 nm. The ratio of the intensity of bright to dark areas of fluorescence in image (b) is ∼2:1.

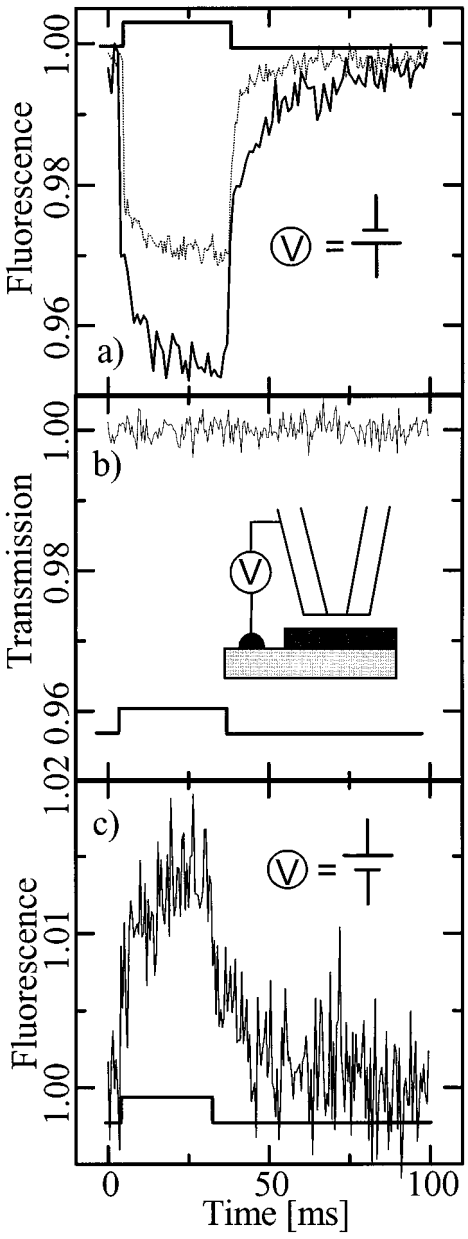

Figure 4. (a) Spatially and time-resolved average NSOM fluorescence intensity changes for ~100 nm thick region of the film(thick-line) and <30 nm thick film (thin-line) of ZnODEP. A 30 ms square electric pulse was applied across the NSOM probe and ITO substrate at 10 Hz (data were collected with 0.5 ms integration steps, 200 integration steps per transient, ~5 min average). The square pulse timing with respect to the fluorescence transient and the polarity of the applied voltage are indicated in the figure. (b) Time-resolved average NSOM transmission intensity changes obtained with the same parameters as in (a). (c) NSOM fluorescence transient obtained with an opposite polarity square pulse as in (a).

position, and/or solid-state structure asymmetry.[32,33] Orbital effects at the central metal atom can also lead to splitting of these bands. The absorption spectrum in Figure 2, does not exhibit an obvious splitting, but a splitting as large as 200 cm^{-1} would be unresolvable.

The corresponding far-field fluorescence spectrum of the nonuniform film and the near-field induced fluorescence spectrum in a 50 nm thick region of the film are also shown in Figure 2. Fluorescence occurs from the lowest excited S_1 state. The near-field fluorescence spectrum represents emission from a thin, single oriented domain and is slightly narrower than the bulk fluorescence spectrum. The far-field emission results from

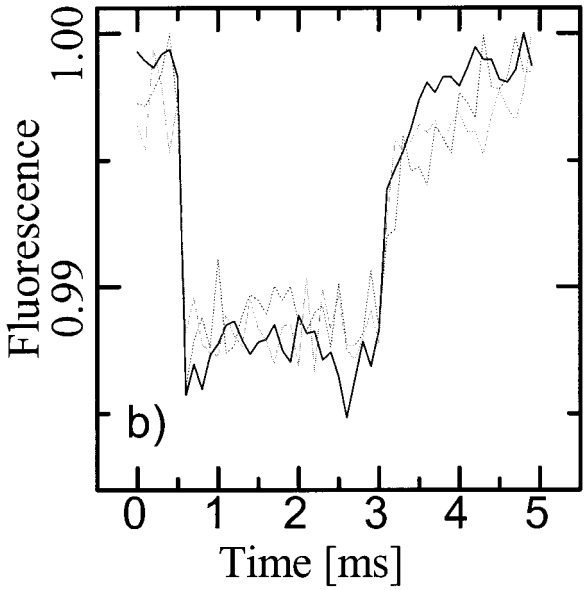

Figure 5. Spatially and time-resolved average fluorescence intensity curves at three different excitation intensity levels (100%, 50%, and 40% of 10 W/cm2). A 2.5 ms square pulse (−5 V) was applied to the NSOM probe at 200 Hz (data were collected with 0.1 ms integration steps, 50 integration steps per transient, ~10 min average).

a distribution of domains, and consequently, the spectrum is slightly broadened. Self-absorption effects in the thicker regions of the film contribute to a decrease in the intensity of the high energy portion of the far-field spectrum. The spectra reveal little evidence of significant perturbation due to aggregation induced spectral shift or quenching.

Topographic, total fluorescence, and polarized fluorescence images (λ_{exc} = 543.5 nm unpolarized) of a 100 nm thin film of ZnODEP on ITO coated glass are shown in Figure 3a−d. The relatively smooth topography shown in Figure 3a is typical for films prepared by pressing two slides that sandwich the ZnODEP together at elevated temperatures. Such films generally display flat upper surfaces with root-mean-square roughness on the order of ~3 nm. The films are comprise multiple domains of a variety of crystalline phases that have been identified by their unique topographic features and fluorescence properties (polarizations, spectra, intensities). Crystalline defects, cracks, and grain and domain boundaries are clearly visible in the topographic image.

The total fluorescence image Figure 3b reveals distinct mesoscopic domains, in which the brighter domains display on average approximately twice the fluorescence intensity as the darker regions. Mesoscopic variations in the fluorescence intensity across the films appears to result from the different effective absorption cross sections at the excitation wavelength and/or different fluorescence quantum yields of distinct crystalline phases and/or crystalline orientations. The images with polarized fluorescence detection (Figure 3c and d) also reveal the mesoscopic domain structure and the highly organized nature of the films. The spatially resolved fluorescence is highly polarized. The polarized fluorescence pattern of the somewhat round region in the upper left portion of Figure 3, parts c and d, is a crystalline disclination point with radial symmetry of the emission dipoles

An NSOM survey of a number of films indicates that the most prevalent film structure contains domains similar to the brighter regions of Figure 3b. Transmission images (not shown) obtained with polarized 400 or 457 nm light display little or no image contrast, whereas the emission is always highly polarized. Highly polarized absorption of light is expected if the plane of

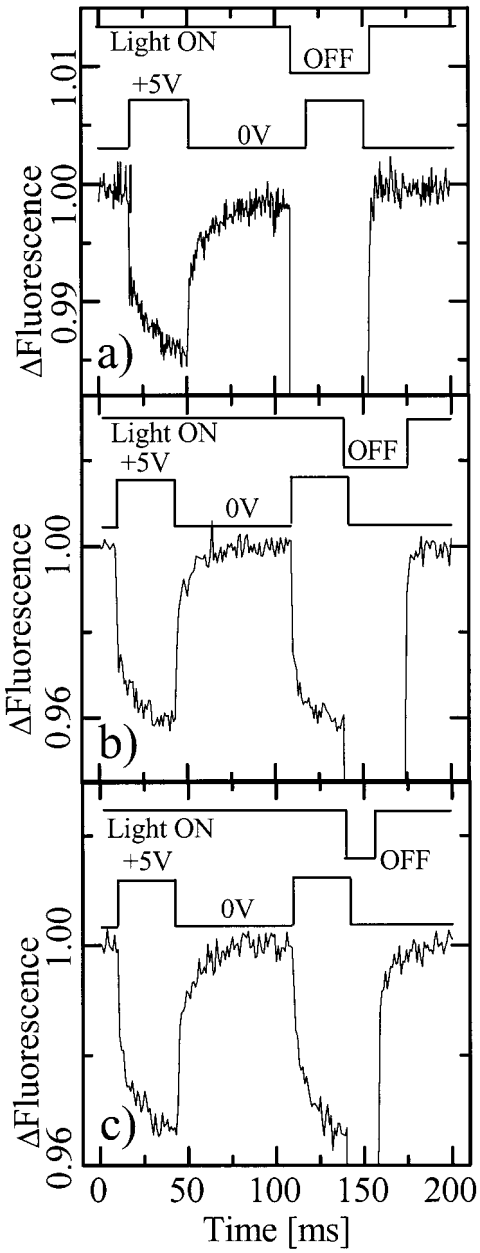

Figure 6. Spatially and time-resolved average fluorescence intensity changes with synchronized light and E-field excitations. The synchronized pulse sequence for the optical and E-fields are shown in the upper portion of the images. The fluorescence transients were collected at 5 Hz and averaged (0.5 ms integration steps, 400 points per transient, 10 min average). A reference trace is recorded in the first 100 ms of transients (a)−(c) where the light is on continuously during the square electric pulse. During the second 100 ms of cycle: (a) the light is off during the square voltage pulse and is then turned on 2 ms after the voltage is turned off (b) the light is ON during most of the square voltage pulse but is turned off 2 ms prior to turning OFF the voltage and then is turned ON 35 ms later (c) the light is ON during most of the square voltage pulse but is turned off 2 ms prior to turning OFF the voltage and then is turned ON 15 ms later. Note the rising region as the light is turned back ON in (a)−(c).

the ZnODEP is perpendicular to the surface or if there is a very large splitting in the energy of the Q or Soret states. The near-degeneracy of the optical absorption in the plane of the ring results in unpolarized absorption.[32] Nearly identical polarized fluorescence NSOM images are obtained when the films are photoexcited with either polarized 400 nm, polarized 457 nm light, or unpolarized 543.5 nm light. Thus, although the NSOM fluorescence images are highly polarized, there is little observed

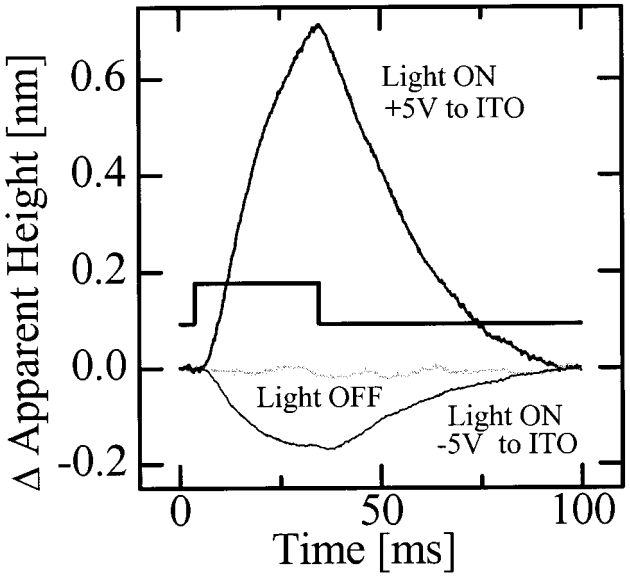

Figure 7. Time-resolved probe−sample distance changes. The square-wave pulse sequence shown in the figure was applied under various conditions as labeled in the figure.

dependence on the polarization of the excitation light. This is further evidence that the absorption process is not highly anistropic.

The apparent discrepancy between the absorption and the fluorescence polarization experiments can be reconciled by a splitting of the degeneracy of the lowest energy Q states in the range 100−200 cm^{-1}. This would be too small to resolve in the far-field absorption experiments but sufficiently large to ensure a large thermal excess in S_1 of the lower polarized Q state. Thus, simultaneous polarized transmission and fluorescence NSOM results obtained at multiple excitation wavelengths suggest that in these domains the plane of the porphyrin ring is oriented parallel or nearly parallel to the plane of the substrate.

E-field Modulated Fluorescence Properties. Spatially and time-resolved near-field fluorescence intensity changes in response to an applied voltage between the probe and the substrate were obtained by parking the NSOM probe over a particular region of the ZnODEP thin film. The results were acquired with shear-force feedback regulation of the probe−sample distance. The fluorescence intensity was recorded as a function of time while the probe/ITO bias was modulated with a repetitive waveform of square wave electric pulses (typically 5V, 30 ms pulse duration) with a repetition rate of 10 Hz. The transients were each subsequently averaged (∼5 min) over each cycle of the waveform to give the average fluorescence transients presented in the figures. The magnitude of the modulated fluorescence signal varied slightly from probe to probe. Probe to probe variations in the surface morphology (Al coating and fiber) would be expected to alter both the spatial variation of the E-field in the probed region and the overlap of the optical and E-fields.

Pitting of the films due to dielectric breakdown was observed by topographic measurements at applied voltages ≥10 V, particularly for extremely thin films (≤50 nm), and for pulse durations exceeding 200 ms. Excess charging of the film at longer pulse durations is apparently responsible for a lower breakdown threshold. *No evidence of pitting was observed in 30−100 nm thick films subjected to 5V, 30 ms pulses, suggesting that dielectric breakdown is a minor factor for these conditions.* For well-ordered regions with few defects, apparent dielectric breakdown often exceeded 10 V.

Typical averaged fluorescence transients recorded for ~100 nm thick region of the film(thick-line) and <30 nm thick film (thin-line) of ZnODEP are shown in Figure 4a. With the ITO charged positive with respect to the Al coated probe (Figure 4a), the fluorescence intensity is quenched by ~3−5% at applied voltages of 5 V. These *positive* ITO *biased* NSOM E-field modulated fluorescence measurements exhibit similar apparent quenching magnitudes to nonspatially resolved measurement of related organic materials with comparable applied fields (i.e., ~0.5−1 MV/cm).[17] However, in contrast to nonspatially resolved measurements, the *negatively biased ITO* NSOM measurements, show *fluorescence increases rather than quenching* as shown in Figure 4c. The increased emission results are apparently not consistent with a simple mechanism of E-field induced dissociation of excitons which can only account for decreased fluorescence intensity in response to an E-field. Greater charge injection into the ZnODEP layer under illumination would be expected for negatively biased ITO vs ITO with a zero bias. The experimental results indicate that a complex set of charge injection, charge transfer, and related processes are also apparently required to explain the data (see the Discussion section).

The average fluorescence transients show two kinetic components: a fast initial change (increase or decrease) in the fluorescence intensity that occurs in less than 0.1 ms (instrument limit) concomitant with the rise of the electric pulse, and a slower change (increase or decrease) that occurs in tens of milliseconds during the electric pulse. As the E-field is switched off, the system recovers with similar kinetics. The intensity dynamics in thin regions of the film (<30 nm) are dominated by the fast component. In film regions of ~100 nm thickness, slow and fast components are of comparable magnitudes, the slow component nearly saturating after ~100 ms. In thicker films, the magnitude of the slow component increases relative to that of the fast component. However, the total magnitudes of the fast and slow progressively decreases until at ~500 nm very little E-Field induced modulation of the fluorescence is observed.

The transmitted light intensity was monitored as a function of time during E-field modulated luminescence experiments. These experiments were designed to check for shifts in the energies of the absorption bands (Stark shifts) in the presence of the E-field, which could potentially account for the observed electromodulated fluorescence properties (modulation of the absorption cross-section). However, E-field effects on the transmitted light intensity are not observed at 400 or 543.5 nm as shown in Figure 4b. The influence of external E-fields on the highly localized electronic energy levels of molecular species is expected to be very small.[15]

The fast kinetic component was investigated by employing 2.5 ms square wave voltage pulses at 200 Hz with 0.1 ms fluorescence integration times per point. Figure 5 shows three normalized average fluorescence transients obtained at three different excitation laser powers ranging from 1 to 10 W/cm^2. Square intensity drops of the same relative magnitude are observed at all laser powers. The fast drop in the fluorescence is instrument-limited, indicating that the E-field induced process occurs on a time scale of less than 0.1 ms. The build up of the slow component in fluorescence trace is almost completely suppressed because the E-field is only on for 2.5 ms.

Simultaneous Modulation of the E-field and Excitation Intensity. Fluorescence NSOM experiments involving synchronized optical and electric pulse sequences were used to probe the photoinduced nature of the slow recovery component of the E-field modulated fluorescence signal. Figure 6a displays the average fluorescence intensity trace of a 100 nm film of ZnODEP and the corresponding optical and electric pulse sequences. During a 200 ms cycle of the electric pulse sequence, two different 5 V square voltage pulses are applied between the probe (negative) and the substrate (positive to ITO). During the first electric pulse the 543.5 nm excitation is on continuously. The laser is turned off just prior to the second electric pulse and is turned on 2 ms after the voltage pulse finishes. The first 100 ms serves as a *reference fluorescence trace* and shows the expected fluorescence quenching during the voltage pulse and recovery of the fluorescence signal after the voltage is turned off. During the second electric pulse, the laser light is off, and consequently, the fluorescence signal goes to zero. As the voltage is turned off, the laser is turned back on, and the fluorescence signal returns to the maximum intensity and shows no evidence of a slow signal recovery. The optical and electrical pulses must be present in order observe the slow component in the recovery of the fluorescence signal. The slow rise component to the fluorescence can be "turned on" by increasing the excitation light level during the "off time" to ~0.1 W/cm^2. These results clearly show that the slow recovery component is a photoinduced process and does not result solely from slow E-field induced effects such as charging of the film in the absence of light. Analogous experiments that probe the slow quenching component during the electric pulse demonstrate that the process is also photoinduced.

The extended time charge trapping behavior of the thin films was investigated by fluorescence NSOM with synchronized optical and electric pulse sequences. Figure 6, parts b and c, display the average fluorescence intensity traces of ~50−100 nm films of ZnODEP and the corresponding optical and electric pulse sequences. The reference fluorescence traces in the first 100 ms regimes of both figures show the expected quenching and recovery of the fluorescence signals in response to the E-field. During the last 100 ms of both sequences, the laser light is turned off 2 ms prior to turning off the voltage and then is turned back on 35 ms and 15 ms later, Figure 6b and c, respectively. In both parts of the figure (6, parts b and c) the fluorescence signal decreases in response to the E-field and goes to zero as the exciting laser light is turned off. The fluorescence signal in Figure 6b shows prompt recovery to maximum intensity as the laser is turned back on, without evidence of a slow component. On the other hand the fluorescence signal shown in Figure 6c shows a slow recovery as the light is turned on. Long time charge trapping behavior is not observed in thin films <~100 nm. Instead, thin films self-discharge in a few tens of milliseconds in the absence of the light.

E-field Modulated Shear-Force Interactions. Apparent topographic changes (z height) in response to the applied E-field were also observed. Transients were collected simultaneously with the fluorescence transients. Figure 7 displays a plot of z height as a function of time under normal operating feedback conditions, for a 50 nm film of ZnODEP under three different conditions. The z displacement is controlled by the shear-forced feedback system and reflects changes in the shear-force probe/sample interaction. No response is detected when a square 5 V pulse of 30 ms duration is applied in the absence of light. However, if the light is on and ITO is charged positive, the probe sample distance *increases* in response to the voltage pulse reaching a maximum of ~7 Å indicating an increase in the probe−sample interaction. If the ITO is negatively charged, the

probe−sample distance *decreases* by ∼2 Å in response to the voltage pulse suggesting a weakening of the probe sample interactions.

The magnitude of the probe−sample distance change varies across the film where different domains give distinctly different topographic responses. In some cases, the magnitude of the topographic response was nearly equivalent for the opposite polarities. The observed topographic response is not an electrical artifact arising from the voltage pulse because 500 nm films do not show an E-field induced probe−sample distance change.

The change in distance between the sample and the probe is not responsible for the observed E-field induced changes in fluorescence. The z displacements in response to the E-field occur much more gradually than the fluorescence changes (fast and slow components). After the rise of the electric pulse, there is an approximately 5−10 ms induction period before the probe−sample distance begins to change that is associated with the time constant of the feedback system. The sensitivity and responsivity of the feedback system can be adjusted resulting in substantially different transient curves than those presented in Figure 7. However, fluorescence transients are virtually unaffected by small changes in the probe sample distance. In one case, the settings of the feedback system were adjusted so that the probe−sample distance did not change in response to the voltage pulses. A fluorescence transient taken under these conditions was identical to that observed under normal feedback conditions.

Discussion

E-Field Modulated NSOM Mechanisms. Field-assisted dissociation of excitons (eq 1) and nonradiative decay (eqs 2 and 3) of singlet excitons by polarons,[14−23] (see the Introduction) cannot alone account for the ZnODEP NSOM data because the fluorescence intensity increases (vs $V = 0$) when the ITO is negatively biased. To explore what other processes might be responsible for the NSOM data, it is important to compare the conditions for the E-field modulated near-field photoluminescence NSOM experiment to the standard nonspatially resolved E-field modulated photoluminescence configuration.

One major difference in the NSOM experiment, is the several orders-of-magnitude higher intensity of irradiation, which produces thousands of excitations per-second-per-molecule. These conditions can lead to a significant steady-state concentration of reversibly formed photogenerated, long-lived species, such as triplet excitons, and certain photooxidation defects. These species are known to act as photoinjected fluorescence quenchers that can be a factor even in the absence of an applied field, such as the $V = 0$ fluorescence NSOM data. *The long-lived photogenerated species can also, in principle, interact with singlet excitons to generate polarons by a "two photon" mechanism which may be an important mechanism for charge generation mechanisms in the NSOM experiment.*

Another important process that should be considered under the high irradiation condition of the NSOM experiment is exciton quenching at the ITO electrodes due to charge injection. This process has been implicated as one of the primary mechanisms for charge separation in organic based photoconductive photocells, optical memory, and electrophotographic applications.[24,35] Exciton migration lengths in organic materials are in the range of 10−500 nm, and consequently, in thin film systems, excitons have a reasonable probability of reaching the electrode.[36] The kinetics of electron versus hole injection at the electrode can be modulated by the applied voltage bias at the electrode.[5,11]

Besides leading to exciton quenching, the charge injection process can lead to a substantial steady-state concentration of charge carriers. The maximum effective charge storage densities in Zn porphyrin films (following charging under illumination and an applied voltage bias) have been measured to be at least 30 μC/cm^2 or 10^{18} charges/cm^3.[25] This corresponds to ∼1000 charges per 5×10^5 molecules of ZnODEP (0.2%) within the photoexcitation volume of a 100 nm aperture near-field probe and a 100 nm thick sample. At the ITO/ZnODEP interface within the excitation volume, there are ∼2000 molecules of ZnODEP (0.4%). The observed ∼5% modulations in the fluorescence intensities are consistent with such charge densities because each polaron should be able to quench the emission of mobile excitons in a large number of surrounding molecules.[15] Photoinduced polaron conduction, which is critical in the charge storing capabilities of ZnODEP, should also be considered for the NSOM experiment.[5,11,12]

Another major difference between the nonspatially resolved E-field modulated fluorescence measurements and the NSOM experiment is that the Al electrode (NSOM probe) is expected to be insulated by a so-called contamination layer, i.e., the ∼5−9 nm gap-between the sample and the probe surfaces (Figure 1c). This should effectively block dc dark- and photocurrents. ac charging of the sample by injection of space charge at the ITO electrode is of course still expected (see Figure 1c). It should be emphasized, however, that the charge-blocking ability of the contamination layer in an NSOM experiment has not been established by experiment. It may be that the probe/sample interface is partially conducting due for example to free ions in the contamination layer and/or sharp protrusions on the NSOM probe which may make intermittent contact.

Finally, the NSOM experiment differs from the usual E-field modulated photoluminescence experiment in the profile of the E-field. As described by Higgins, the E-field in the vicinity of an electrically biased Al coated, optical fiber NSOM probe is highly inhomogeneous, with much greater intensity at the edges of the NSOM aperture.[10] This leads to a significant lateral component of the field, i.e., parallel to the plane of the sample. In principle, the inhomogeneous field could lead to a substantial lateral polarization of the distribution of polarons, which in turn could alter the balance of negative and positive polarons in the region of the sample most effectively probed by the NSOM optical field (i.e., immediately under the aperture).

Considering the large number of potential processes, the complexity of these processes, and the limited available data, it is not possible to unequivocally establish a comprehensive model for the E-Field modulated NSOM data. In particular, the increase in fluorescence in a negatively biased configuration versus $V = 0$ is difficult to explain. The increase in fluorescence with negatively biased ITO could be due to injection of negative polarons, which have been reported to deplete the concentration of charged quenching defects by a redox mechanism.[18] High excitation rates in the NSOM experiments, as described above, could be responsible for a substantial steady-state concentration of photogenerated fluorescence quenching defects and photoinjected charges for the $V = 0$ configuration. Thus, the fluorescence yield at $V = 0$ may be reduced from the yield of a negatively ITO biased material, as described above. The putative imbalance of negative and positive polaron concentrations in the probed region due to E-field inhomogeneity may be another important factor in leading to different polaron/exciton quenching kinetics and efficiencies for positively and negatively biased ITO electrodes. Apparently, the positive polarons are substantially more effective exciton quenchers than

the negative polarons. Furthermore, there may be a diode-like behavior for charge separation at the organic/ITO junction.

Two distinct rates of charging/discharging of the device equivalent structure are revealed in the electromodulated fluorescence traces shown in Figure 4. The electrode/ZnODEP interfacial region is expected to charge/discharge simultaneously with the application/removal of the voltage (<1 ns rise time of the square voltage pulse). The observed time of the slow component (quenching or recovery) in the fluorescence traces is consistent with the time necessary for charging and discharging of the film by photoconduction. In actual charge trapping devices based on 1 μm films of ZnODEP, stored charges are nearly completely released from the ZnODEP layer within ~1 s, when illuminated with laser powers of ~0.1 mW/cm^2 under short circuit conditions.[11] The release of stored charges in these studies was measured by short-circuit photocurrent measurements.

In the present experiments, the time necessary for complete discharging of the thin ZnODEP layer (<100 nm) at 0 applied volts, as measured by the slow recovery of the fluorescence signal, is ~25−50 ms at excitation intensities of 1 W/cm^2. The movement of polarons within the ZnODEP layer involves photoconduction and is therefore dependent on the excitation intensity and the magnitude of the applied voltage and is expected to proceed at a slower rate.[11] The observed fast response of the fluorescence signal occurs in less than the instrument limit of 0.1 ms concomitant with the rise or fall of the voltage pulse. The fast component of exciton quenching is assigned to both quenching by positive polarons and electron-transfer quenching at the organic/ITO interface.

The electromodulated fluorescence signal is not excitation power dependent over the range 1−10 W/cm^2. The slow response of the fluorescence signal (during the voltage pulse or after its removal) arises from a photoinduced process within the ZnODEP layer and displays an excitation power dependence requiring at least 0.1 W/cm^2 to be observed in our experiments. The slow response can be suppressed by either reducing the light intensity and/or utilizing the very short electric pulses. In thin films, <30 nm, the relative magnitude of the slow component is diminished, indicating that the electromodulated signal is dominated by the exciton interactions at the interface. As film thicknesses increase, it is generally observed that the magnitude of the slow kinetic component increases as a result of moving charges deeper into the film away from the interfacial region. In this case, a larger fraction of excitons interact with charges deeper in the film and may not migrate to the interface.

Electromodulated Probe/Sample Interactions. The shear-force feedback system modulates the probe sample distance in order to maintain constant probe dither amplitude at the driving frequency.[37] In the absence of an applied E-Field, the dither amplitude of the near-field probe is believed to be sensitive primarily to shear forces in the "impurity layer" at the surface, which increase as the sample distance is reduced. The experimentally observed response of the shear-force feedback system to simultaneous E-fields and NSOM optical excitation suggests that charges in the near field region are altering the shear-forces. In principle, photoinduced charges in the near field region should increase the probe/sample Coulomb forces leading to probe retraction in feedback. This is indeed observed when the bias on ITO is changed from $V = 0$ to a positive bias.

The opposite effect, however, is observed when ITO is changed from $V = 0$ to a negative bias, which should also increase charging in an opposite but analogous manner, see the Results section. It may be that this unexpected effect is not simply a result of probe/sample Coulomb interactions. Perhaps other processes are operating, such as tip/sample electrical breakdown and/or charge induced modifications in the physical properties and/or organization of the impurity layer, sample surface, and/or probe surface. Indeed, experiments analogous to those shown in Figure 7 for a different materials, namely the conjugated polymer MEH−PPV, reveal an intermittence and tip/sample distance dependence that are consistent with electrical discharge being a factor in the apparent response of the shear-force feedback system to an applied E-field at the NSOM probe.[38]

Conclusions

The concentrated electric field (E-field) in the vicinity of a *voltage-biased* near-field optical probe is used to modulate the photoluminescence and probe/sample shear-force of bilayers of the photoconductive charge-trapping material ZnODEP. The results suggest that the technique has indirectly monitored the local (50−100 nm) concentration of photoinduced charge carriers, although a quantitative model has not yet been formulated. The observed phenomena may be the basis of a new scanning probe technique for spatially resolving charge densities and photoinduced charge injection in functional devices and device prototypes that are based on organic materials. One feature of the data, namely the unexpected increase in fluorescence intensity for negative ITO biases, remains puzzling.

Acknowledgment. We gratefully acknowledge helpful discussions with Prof. Dan Higgins. This research was supported by the National Science Foundation and the Robert A. Welch Foundation. We thank Don O'Connor and Jason McNeill for helpful discussions.

References and Notes

(1) For a recent overview, see "Special Issue on Molecular Materials in Electronic and Optoelectronic Devices" in *Acc. Chem. Res*., vol 32(3), **1999**.

(2) Adams, D. M.; Kerimo, J.; Olson, E. J. C.; Zaban, A.; Gregg, B. A.; Barbara, P. F. *J. Am. Chem. Soc.* **1997**, *119*, 10 608.

(3) Conboy, J. C.; Olson, E. J. C.; Adams, D. M.; Kerimo, J.; Zaban, A.; Gregg, B. A.; Barbara, P. F. *J. Phys. Chem. B* **1998**, *102*, 4516.

(4) Barbara, P. F.; Adams, D. M.; O'Connor, D. B. *Annu. Rev. Mater. Sci.* **1999**, *29*, 433−469.

(5) Liu, C. Y.; Bard, A. J. *Acc. Chem. Res.* **1999**, *32*, 235−245.

(6) Gao, Y. *Acc. Chem. Res.* **1999**, *32*, 247−255.

(7) Alvarado, S. F.; Libioulle, L.; Seidler, P. F. *Synth. Met.* **1997**, *91*, 69−72.

(8) Kelley, T. W.; Granstrom, E. L.; Frisbie, C. D. *Adv. Mater*. **1999**, *11*, 261−264.

(9) Hu, J.; Odom, T. W.; Lieber, C. M. *Acc. Chem. Res.* **1999**, *32*, 435−445.

(10) Mei, E.; Higgins, D. A. *J. Phys. Chem. A* **1998**, *102*, 7558−7263.

(11) Liu, C. Y.; Pan, H. L.; Fox, M. A.; Bard, A. J. *Chem. Mater*. **1997**, *9*, 1422−1429.

(12) Liu, C. Y.; Pan, H. L.; Fox, M. A.; Bard, A. J. *Science* **1993**, *261*, 897−899.

(13) Moerner, W. E.; Plakhotnik, T.; Irngartinger, T.; Wild, U. P.; Pohl, D. W.; Hecht, B. *Phys. Rev. Lett.* **1994**, *73*, 2764−2767.

(14) Popovic, Z. D.; Khan, M. I.; Atherton, S. J.; Hor, A. M.; Goodman, J. L. *J. Phys. Chem. B* **1998**, *102*, 657−663.

(15) Kalinowski, J.; Stampor, W.; Di Marco, P. *J. Electrochem. Soc.* **1996**, *143*, 315−325.

(16) Stampor, W.; Kalinkowski, J.; Di Marco, P.; Fattori, V. *Appl. Phys. Lett.* **1997**, *70*, 1935−1937.

(17) Deussen, M.; Scheidler, M.; Bassler, H. *Synth. Met.* **1995**, *73*, 123−129.

(18) Dyreklev, P.; Inganas, O.; Paloheimo, J.; Stubb, H. *J. Appl. Phys.* **1992**, *71*, 2816−2820.

(19) Vissenberg, M. C. J. M.; de Jong, M. J. M. *Phys. Rev. B* **1998**, *57*, 2667−2670.

(20) Ziemelis, K. E.; Hussain, A. T.; Bradley, D. D. C.; Friend, R. H.; Ruhe, J.; Wegner, G. *Phys. Rev. Lett.* **1991**, *66*, 2231−2234.

(21) Moses, D.; Okumoto, H.; Lee, C. H.; Heeger, A. J.; Ohnishi, T.; Noguchi, T. *Phys. Rev. B* **1996**, *54*, 4748−4754.
(22) Deussen, M.; Bolivar, P. H.; Wegmann, G.; Kurz, H.; Bassler, H. *Chem. Phys.* **1996**, *207*, 147−157.
(23) Tasch, S.; Kranzelbinder, G.; Leising, G.; Scherf, U. *Phys. Rev. B.* **1997**, *55*, 5079−5083.
(24) Gregg, B. A.; Fox, M. A.; Bard, A. J. *J. Phys. Chem.* **1990**, *94*, 1586−1598.
(25) Liu, C. Y.; Hasty, T.; Bard, A. J. *J. ElectroChem. Soc.* **1996**, *143*, 1914−1918.
(26) Gregg, B. A.; Fox, M. A.; Bard, A. J. *J. Am. Chem. Soc.* **1989**, *111*, 3024−3029.
(27) Vanden Bout, D. A.; Kerimo, J.; Higgins, D. A.; Barbara, P. F. *J. Phys. Chem.* **1996**, *100*, 11 843−11 849.
(28) Higgins, D. A.; Vandenbout, D. A.; Kerimo, J.; Barbara, P. F. *J. Phys. Chem.* **1996**, *100*, 13 794−13 803.
(29) Higgins, D. A.; Kerimo, J.; Vandenbout, D. A.; Barbara, P. F. *J. Am. Chem. Soc.* **1996**, *118*, 4049−4058.
(30) Reid, P. J.; Higgins, D. A.; Barbara, P. F. *J. Phys. Chem.* **1996**, *100*, 3892−3899.
(31) Betzig, E.; Trautman, J. K. *Science* **1992**, *257*, 189−195.
(32) Gouterman, M. *J. Chem. Phys.* **1959**, *30*, 1139−1161.
(33) Gouterman, M. *J. Mol. Spectrosc.* **1961**, *6*, 138−163.
(34) Gregg, B. A.; Fox, M. A.; Bard, A. J. *J. Phys. Chem.* **1989**, *93*, 4227−4234.
(35) Gregg, B. A. *J. Phys. Chem.* **1996**, *100*, 852−859.
(36) Adams, D. M.; Kerimo, J.; O'Connor, D. B.; Barbara, P. F. *J. Phys. Chem. A* **1999**, *103*, 10 138−10 143.
(37) Betzig, E.; Finn, P. L.; Weiner, J. S. *Appl. Phys. Lett.* **1992**, *60*, 2484.
(38) McNeill, J. D.; O'Connor, D. B.; Kämmer, S. B.; Barbara, P. F. *in preparation* **2000**.